ACS APPLIED MATERIALS & INTERFACES

LETTER

www.acsami.org

On the Secondary Droplets of Self-Running Gallium Droplets on GaAs Surface

Jiang Wu,[†] Zhiming M. Wang,*[,†,‡] Alvason Z. Li,[†] Mourad Benamara,[†] and Gregory J. Salamo[†]

[†]Institute for Nanoscale Materials Science and Engineering, University of Arkansas, Fayetteville, Arkansas 72701, United States

[‡]State Key Laboratory of Electronic Thin Films and Integrated Devices, University of Electronic Science and Technology of China, Chengdu 610054, P. R. China

ABSTRACT: Self-running droplets by thermal evaporation GaAs (001) surface are studied and analyzed using a scanning electron microscope. The sample is prepared under high-temperature annealing in an ultrahigh vacuum molecular beam epitaxy system. Particularly, secondary droplets which formed along primary droplet running trails are investigated. The secondary droplets are found to initially move along the $[1\bar{1}0]$ instead of [110] direction, but these droplets tend to turn into [110] direction as they grow bigger. The scanning electron microscope also captures nanoscale footprints of secondary droplets different from the main droplets.

KEYWORDS: droplet, GaAs, scanning electron microscopy, epitaxy, surface

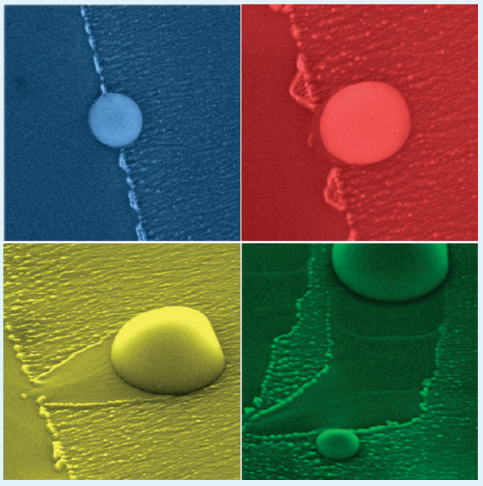

Droplets have attracted a lot of attention for many years because of their practical applications in various areas, including epitaxy growths, lab-on-a-chip techniques, and microfluidic systems.[1−4] In the last 10 years, droplet epitaxy technique has brought pronounced control of nanostructure designs and manipulations.[5−9] Novel quantum rings, quantum dot pairs, quantum molecules, nanoholes, etc., grown by droplet epitaxy open opportunities for a new generation of optoelectronic and electronic devices.[10−17] As a result, development of droplet epitaxy technique has led to a resurgence of interest in metallic droplets.[18,19] Very recently, Tersoff et al. and Hilner et al. have reported innovative studies of Ga droplets formed on GaAs and GaP surfaces by high-temperature annealing in a vacuum.[20,21] Such observations open opportunities to steer formation and motion of droplets and, more importantly, to form large scale ordering for technical applications, such as droplet epitaxy. So far, all the works on self-running droplets have been devoted to the "mother" droplet and a detailed picture of the "daughter" droplet resulting from the thermal evaporation on a GaAs surface is still lacking. Here, the "mother" or primary droplets refer to the droplets initially formed on the GaAs surface, whereas "daughter" or secondary droplets refer to the droplets formed from the footprints of primary droplets.

In this paper, secondary droplets formed along the trail of main running droplet are reported. The detailed formation of secondary Ga droplets and the self-driven motion of droplets are investigated using a scanning electron microscope (SEM) and an atomic force microscope (AFM). For the first time, "daughter" droplets are observed to move along the $[1\bar{1}0]$ direction. Our observation has also demonstrated that droplets prefer to form along the boundary between a clean GaAs surface and a "mother" droplet trail. If the substrate were patterned, ordered droplets would be created by using this method. More interestingly, the "daughter" droplets are observed to turn into [110] direction when they grow bigger. In addition, distinct nanoscale footprints are observed for these "daughter" droplets. The main focus of this study is on the evolution of running daughter droplets and their nanoscale footprints during high-temperature annealing.

A semi-insulating epitaxial ready GaAs (001) sample is prepared in a MBE chamber. Thermal oxide desorption is carried out at 600 °C for ten minutes. Following the oxide desorption, a 500 nm thick GaAs buffer layer is epitaxially grown at 580 °C. Sequentially, all the source cells are closed and the substrate temperature is ramped up immediately to 680 °C with a ramp rate of 50 °C/minute under high vacuum of 1×10^{-8} Torr. This high temperature is maintained for 10 min for desorption of As and formation of Ga droplets. Subsequently, the substrate is cooled down to room temperature and sample surface analysis is carried out by microscopy techniques.

Received: May 2, 2011
Accepted: May 16, 2011
Published: May 19, 2011

All the previous reports on self-running droplets have shown that droplets prefer to move along particular direction due to surface anisotropic properties.[20−22] For example, Ga droplet tends to move along [110] or [1$\bar{1}$0] direction on GaAs (001) surface. However, this observation holds true as long as a homogeneous surface is used. Figure 1 displays SEM images of secondary droplets forming along the trail of a main droplet. An interesting observation is that the secondary droplet movement is along [1$\bar{1}$0] direction which is perpendicular to the trail of primary droplets. Analogous to primary droplets, the driving force can also be related to three major factors: (1) the nonequilibrium surface energy of the surrounding surface; (2) surface roughness introduced force; (3) gradient in the thermodynamic free energy underneath a droplet.[20,21,23] Compared with primary droplets, the unique formation scenario of secondary droplets is attributed to the unusual motion along [1$\bar{1}$0] direction. First, even though the surface anisotropy confines the droplet motion along [110] direction, the primary droplet trail brings in a nonequilibrium surface energy difference along [1$\bar{1}$0] direction for secondary droplets. Second, the secondary droplets forming along the trail experience an immediate surface roughness contrast; Since the primary droplet trail is formed along [110], the secondary droplet certainly has a smooth surface and a rough surface on its two sides along [1$\bar{1}$0] direction at the very beginning of droplet formation. Last but not least, even though no direct evidence of different directions of free energy gradient can be provided, we have found indirect evidence that the free energy gradient under a droplet also plays a significant role in the motion behavior of secondary droplets, which will be discussed in a later section. Another interesting feature worth pointing out is that the angle of the secondary droplet trail is much larger than the primary droplet trail as indicated in Figure 1. The primary droplet size has been found to increase slowly while moving. We assume an empirical linear relationship of droplet size and trail length as $D_1 = (1 + \alpha L)D_0$. Here, D_0 and D_1 are the initial diameter and finial diameter of droplets, respectively, L is the trail length, and α is the factor related to surface properties, which govern how fast droplets grow. The factor α is as small as 0.039 μm^{-1} for the primary droplets, whereas it is ~1.0 μm^{-1} for the secondary droplets. Such huge difference can be explained by the surface anisotropy. Because of a higher energy barrier for Ga diffusion along [1$\bar{1}$0], the primary droplets are more confined and the diameter change is expected to be small. On the contrary, the secondary droplets are pushing to move along the [1$\bar{1}$0] direction, but they still prefer to diffuse along [110] direction. Moreover, motion of a droplet along [1$\bar{1}$0] is slower compared to [110] and the droplet diameter shows a high increase ratio given a same droplet displacement distance and growth rate. Therefore, a large trail angle θ is expected for droplets moving along the [1$\bar{1}$0] direction, as shown in Figure 1b.

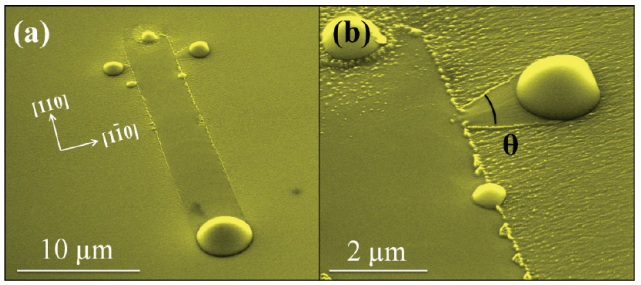

Figure 1. (a) Self-running Ga droplet with secondary droplets nucleation on the trail edge. (b) Magnified SEM image of a running secondary droplet.

The evolution of "mother" droplet formation has been demonstrated by recent studies.[20,21] In order to understand the underlying mechanisms of running droplets as well as controlling and ordering droplets, studying the evolution of droplet formation is essential. We now discuss the evolution of secondary droplets. We captured various stages from different secondary droplets, and are able to assemble the evolution processes of secondary droplets. As shown on Figure 2, the detail historical evolution steps are: (a) when droplet diameter is in the range below 500 nm, droplets stick on the original primary trail boundary; (b) when droplet diameter reaches about 500 nm, it starts to move along the [1$\bar{1}$0] direction; (c) while the droplet is growing up, its trial is also broadening out; (d) when the droplet is as big as 2000 nm in diameter, it starts to turn its moving direction 90° (or less) to the [110] direction. The initial formation of secondary droplets along primary droplet trail edge is due to a higher evaporation rate along the primary droplet trail edges. This high evaporation can be further understood by a high density of miscuts along the trail edges.[22]

The presence of miscuts lowers the congruent evaporation temperature and thus enhances the decomposition of GaAs at the region of miscuts.[22] Similar to ref 22 ,the trail edges of primary droplets are such region with superior evaporation rate. By intentionally creating these high-density miscuts by lithography, ordered droplets are expected to be formed by thermal evaporation. The secondary running droplets are found to move with a much smaller size than that of primary droplets. Such observation confirms the affects of surface properties on the

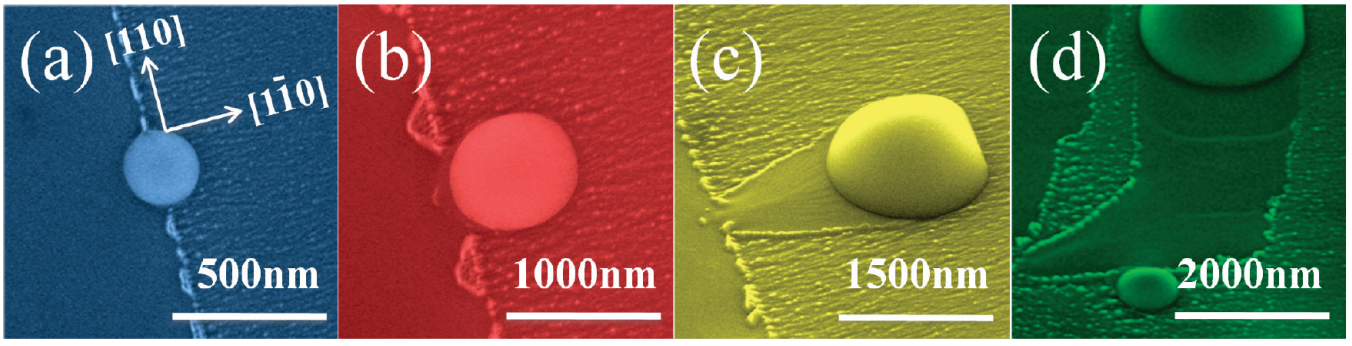

Figure 2. Sequential images captured for different secondary droplets. (a) Nucleation of a secondary droplet at the boundary of a primary droplet trail; (b) breakout of a secondary droplet; (c) a moving secondary droplet; (d) a secondary droplet makes a turn.

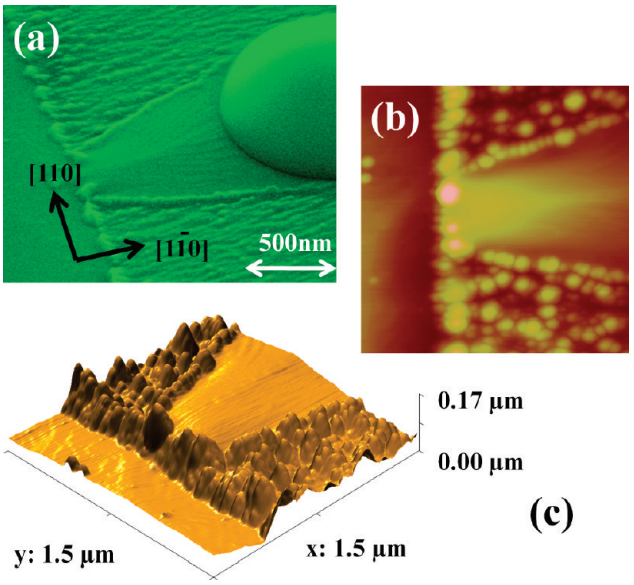

Figure 3. (a) SEM image of a self-runing secondary droplet; (b) AFM image of a secondary droplet trail; (c) three-dimensional AFM image of a secondary droplet trail.

driving forces. Since a high contract of surface energy and surface roughness has been presented initially, the total driving force put on a secondary droplet is expected to be higher than that of a primary droplet at the very beginning of droplet formation. It is worth to mention that both the evaporation force and surface roughness introduced force are in the direction of [1$\bar{1}$0] due to the presentence of the primary trail. Therefore, the forces temporarily overcome the energy barrier along [1$\bar{1}$0] and lead to motion in this direction. Another fascinating observation is that secondary droplets can turn to [110] direct when the droplet size is big enough. As shown in Figure 2c, the secondary droplet has a flat frontage and a circular rear, which indicate that the droplet is restrained in the [1$\bar{1}$0] direction. After the droplet size increases, forces pointing to [1$\bar{1}$0] direction are offset by surface anisotropy. Similar to primary droplets, the secondary droplets can be displaced to ±[110] direction upon fluctuations and then the secondary droplets would start to move along [110] direct and have same behavior as a primary droplet.

As secondary droplets move away from the primary droplet trail, surface steps form behind a secondary droplet and are ordered differently from primary droplet trail steps. Figure 3 shows the AFM and SEM images of the footprints of a secondary droplet. Although trails from both primary droplets and secondary droplets have smooth surfaces, the trails formed behind a secondary droplet do not show any periodic patterns until it changes its running direction to [110]. The periodic patterns of primary droplets are indication of stick−slip type of motion, which alternates between sticking and sliding states. Therefore, this observation indicates continuous sliding motion of secondary droplets instead of stick−slip type of motion. The typical nanoscale terraces formed by a primary droplet and secondary droplet are shown in Figure 4. Figure 4a shows the nanoscale steps ordered by a secondary droplet. Unlike the footprints of a primary droplet shown in Figure 4b, the step orientation is more perpendicular to the droplet. However, both the terraces from a secondary droplet and primary droplet show almost same orientation relative to the GaAs crystal structure. Therefore, it

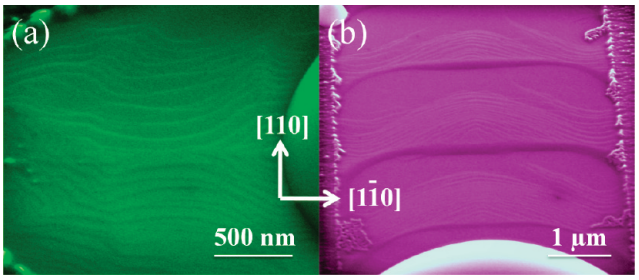

Figure 4. SEM image of the nanoscale terraces of (a) a secondary droplet and (b) a primary droplet.

is safe to conclude that the ordering of nanoscale terraces is not related to the moving direction of droplets but to the substrate crystal structure. Therefore, it can be derived that the forces due to thermodynamic free energy gradient on a secondary droplet would have a same direction, which is along [110]. Because the motion of a secondary droplet is moving along [1$\bar{1}$0] and the terraces are symmetric relative to the droplet, the force along −[110] and +[110] are equal and not affecting the motion of a secondary droplet until it turns to [110] direction. Therefore, the droplets are mainly propelled by surface roughness and free energy difference of droplet surrounding, which explains why no periodic terrace is observed as secondary droplets moving along the [1$\bar{1}$0] direction.

In conclusion, we present experimental observation of running "daughter" droplets on GaAs (001) surface. By using SEM and AFM techniques, the formation of running droplets is identified to be different between primary and secondary droplets. The motion of secondary droplets is analyzed in details. Furthermore, we obtain secondary droplet evolution sequences and add essential information to understand droplet self-motion of Ga droplets on GaAs surface. Moreover, the nanoscale footprints of secondary droplets are presented for the first time. The study of secondary droplets suggests that steer droplet can be possible by prepatterning the surface. Finally, as the secondary droplets prefer to nucleate to boundary of the primary trails, large-scale ordering of droplets is possible to advance droplet epitaxy technique.

AUTHOR INFORMATION

Corresponding Author
*E-mail: zmwang@uark.edu.

ACKNOWLEDGMENT

This work was funded by MRSEC Program of NSF Grant DMR-0520550.

REFERENCES

(1) Heyn, C.; Stemmann, A.; Köppen, T.; Strelow, C.; Kipp, T.; Grave, M.; Mendach, S.; Hansen, W. *Nanoscale Res. Lett.* **2010**, *3*, 576–580.
(2) Li, A. Z.; Wang, Z. M.; Wu, J.; Xie, Y.; Sablon, K. A.; Salamo, G. J. *Cryst. Growth Des.* **2009**, *6*, 2941–2943.
(3) Baroud, C. N.; Gallaire, F.; Dangla, R. *Lab Chip* **2010**, *10*, 2032–2045.
(4) Richardson, H. H.; Carlson, M. T.; Tandler, P. J.; Hernandez, P.; Govorov, A. O. *Nano Lett.* **2009**, *3*, 1139–1146.
(5) Lee, J. H.; Wang, Z. M.; Kim, E. S.; Kim, N. Y.; Park, S. H.; Salamo, G. J. *Nanoscale Res. Lett.* **2009**, *2*, 308.

(6) Wu, J.; Shao, D.; Dorogan, V. G.; Li, A. Z.; Li, S.; Decuir, E. A.; Manasreh, M. O.; Wang, Z. M.; Mazur, Y. I.; Salamo, G. J. *Nano Lett.* **2010**, *4*, 1512–1516.
(7) Somaschini, C.; Bietti, S.; Koguchi, N.; Sanguinetti, S. *Nano Lett.* **2009**, *10*, 3419–3424.
(8) Wang, Z. M.; Liang, B.; Sablon, K. A.; Lee, J.; Mazur, Y. I.; Strom, N. W.; Salamo, G. J. *Small* **2007**, *2*, 235–238.
(9) Alonso-Gonzãlez, P.; Gonzãlez, L.; Martãn-Sãnchez, J.; Gonzãlez, Y.; Fuster, D.; Sales, D.; Hernãndez-Maldonado, D.; Herrera, M.; Molina, S. *Nanoscale Res. Lett.* **2010**, *12*, 1913–1916.
(10) Mano, T.; Kuroda, T.; Mitsuishi, K.; Yamagiwa, M.; Guo, X.; Furuya, K.; Sakoda, K.; Koguchi, N. *J. Cryst. Growth* **2007**, 740–743.
(11) Liang, B.; Wang, Z.; Wang, X.; Lee, J.; Mazur, Y. I.; Shih, C.; Salamo, G. J. *ACS Nano* **2008**, *11*, 2219–2224.
(12) Li, S.; Abliz, A.; Yang, F.; Niu, Z.; Feng, S.; Xia, J.; Hirose, K. *J. Appl. Phys.* **2003**, *8*, 5402.
(13) Sablon, K. A.; Lee, J. H.; Wang, Z. M.; Shultz, J. H.; Salamo, G. J. *Appl. Phys. Lett.* **2008**, *20*, 203106.
(14) Li, S.; Xia, J. *Appl. Phys. Lett.* **2007**, *9*, 092119.
(15) Wu, J.; Li, Z.; Shao, D.; Manasreh, M. O.; Kunets, V. P.; Wang, Z. M.; Salamo, G. J.; Weaver, B. D. *Appl. Phys. Lett.* **2009**, *17*, 171102.
(16) Bietti, S.; Somaschini, C.; Koguchi, N.; Frigeri, C.; Sanguinetti, S. *Nanoscale Research Letters* **2010**, *12*, 1905–1907.
(17) Wang, Z. M.; Holmes, K.; Shultz, J. L.; Salamo, G. J. *Phys. Status Solidi A* **2005**, *8*, 1339–1339.
(18) Wu, J.; Wang, Z. M.; Li, A. Z.; Li, S.; Salamo, G. *Phys. Status Solidi (RRL)* **2010**, *12*, 371–373.
(19) Li, A. Z.; Wang, Z. M.; Wu, J.; Salamo, G. J. *Nano Res.* **2010**, *7*, 490.
(20) Hilner, E.; Zakharov, A. A.; Schulte, K.; Kratzer, P.; Andersen, J. N.; Lundgren, E.; Mikkelsen, A. *Nano Lett.* **2009**, *7*, 2710–2714.
(21) Tersoff, J.; Jesson, D. E.; Tang, W. X. *Science* **2009**, *5924*, 236–238.
(22) Tersoff, J.; Jesson, D. E.; Tang, W. X. *Phys. Rev. Lett.* **2010**, *3*, 035702.
(23) Chaudhury, M. K.; Whitesides, G. M. *Science* **1992**, *5063*, 1539–1541.